Diffusely Bound Mg^{2+} Ions Slightly Reorient Stems I and II of the Hammerhead Ribozyme To Increase the Probability of Formation of the Catalytic Core†

David Rueda,‡ Katrin Wick,‡ S. Elizabeth McDowell,§ and Nils G. Walter*,‡

Department of Chemistry and Biophysics Research Division, The University of Michigan, 930 North University Avenue, Ann Arbor, Michigan 48109-1055

Received May 12, 2003; Revised Manuscript Received June 24, 2003

ABSTRACT: The hammerhead ribozyme is one of the best-studied small RNA enzymes, yet is mechanistically still poorly understood. We measured the Mg^{2+} dependencies of folding and catalysis for two distinct hammerhead ribozymes, HHL and HHα. HHL has three long helical stems and was previously used to characterize Mg^{2+}-induced folding. HHα has shorter stems and an A·U tandem next to the cleavage site that increases activity ∼10-fold at 10 mM Mg^{2+}. We find that both ribozymes cleave with fast rates (5−10 min^{-1}, at pH 8 and 25 °C) at nonphysiologically high Mg^{2+} concentrations, but with distinct Mg^{2+} dissociation constants for catalysis: 90 mM for HHL and 10 mM for HHα. Using time-resolved fluorescence resonance energy transfer, we measured the stem I−stem II distance distribution as a function of Mg^{2+} concentration, in the presence and absence of 100 mM Na^+, at 4 and 25 °C. Our data show two structural transitions. The larger transition (with Mg^{2+} dissociation constants in the physiological range of ∼1 mM, below the catalytic dissociation constants) brings stems I and II close together and is hindered by Na^+. The second, globally minor, rearrangement coincides with catalytic activation and is not hindered by Na^+. Additionally, the more active HHα exhibits a higher flexibility than HHL under all conditions. Finally, both ribozyme−product complexes have a bimodal stem I−stem II distance distribution, suggesting a fast equilibrium between distinct conformers. We propose that the role of diffusely bound Mg^{2+} is to increase the probability of formation of a properly aligned catalytic core, thus compensating for the absence of naturally occurring kissing-loop interactions.

Hammerhead ribozymes are found in a number of plant pathogenic viroids and virusoids, where they are involved in self-cleavage and self-ligation of the plus and minus strands during the pathogen's genome replication (*1*, *2*). In addition, the hammerhead ribozyme has been found to mediate self-cleavage of satellite DNA transcripts in the newt (*3*). Several hammerhead crystal structures have been determined (*4*−*6*), and the global structure was confirmed in solution by steady-state fluorescence resonance energy transfer (FRET)[1] (*7*, *8*), gel electrophoresis (*9*), and transient electric birefringence (*10*) (Figure 1). The ribozyme consists of three helical stems arranged in a "Y-shape", with 11 nucleotides at the junction forming the highly conserved catalytic core (*11*, *12*) (Figure 1). The catalytic core is comprised of two domains; stems I and II are arranged in an acute angle by a sharp uridine turn in the backbone trajectory of domain 1, while stems II and III stack coaxially with the formation of two G·A and one A·U non-Watson−Crick base pairs in domain 2. The cleavage site is located 3′ to C17, which is buttressed to domain 1 by a single hydrogen bond with C3 (Figure 1).

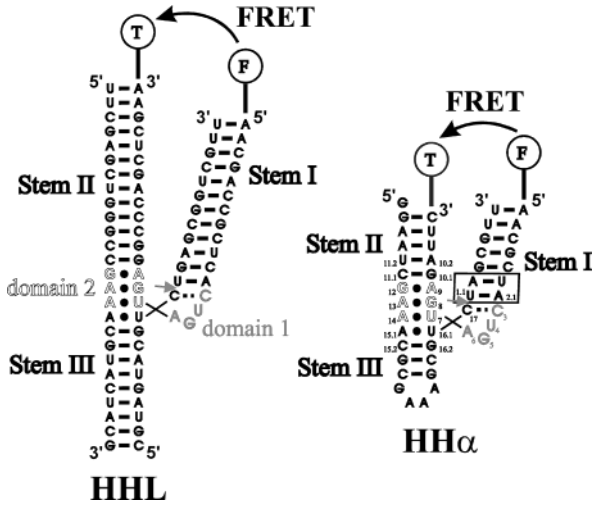

FIGURE 1: Secondary structure of the hammerhead ribozyme constructs, HHL and HHα, used in this study. The cleavage site is marked with an arrow. The catalytic core bases of domain 1 are marked in gray, and those of domain 2 are highlighted with outlined letters. The 5′ end of stem I and the 3′ end of stem II are labeled with fluorescein (F) and tetramethylrhodamine (T), respectively, which act as a FRET pair in our tr-FRET experiments. The box on HHα indicates the A·U tandem that accelerates cleavage (*25*). Bases are numbered according to ref *52*.

† This work was supported by NIH Grant GM62357-01 to N.G.W., a postdoctoral fellowship from the Swiss National Funds to D.R., a DAAD scholarship to K.W., and a University of Michigan Biophysics fellowship to S.E.M.

* To whom correspondence should be addressed. Phone: (734) 615-2060. Fax: (734) 647-4865. E-mail: nwalter@umich.edu.

‡ Department of Chemistry.

§ Biophysics Research Division.

[1] Abbreviations: FRET, fluorescence resonance energy transfer; fwhm, full width at half-maximum; HPLC, high-performance liquid chromatography; NLPB, nonlinear Poisson−Boltzmann; NMR, nuclear magnetic resonance; tr-FRET, time-resolved fluorescence resonance energy transfer.

10.1021/bi0347757 CCC: $25.00
Published on Web 07/30/2003

The crystal structures of the hammerhead ribozyme have played a significant role in understanding the overall structure of the active conformation. There is, however, considerable controversy due to inconsistencies between the crystal structures and some of the biochemical studies (*13*). In particular, the crystal structure shows near A-type backbone geometry around the scissile phosphate, a structure unsuited for the S_N2-type in-line attack mechanism proposed for the reaction. Likewise, the exocyclic groups of G5 are exposed to solvent in the crystal structure, while their modification results in a loss of catalytic activity of 2−3 orders of magnitude (*13*). Moreover, the *pro-*R_p oxygens of the phosphates of A9 and the cleavage site are approximately 20 Å apart in the crystal structure, while sulfur modification interference experiments and rescue with thiophilic metal suggest that these two sites coordinate the same metal ion in the transition state (*14*). It has therefore been proposed that the hammerhead ribozyme must undergo a conformational change from the crystal structure to reach its catalytically active structure. The extent of this conformational change is still a matter of debate (*14*−*16*). Crystallographic evidence suggests that, at the very least, the C17·C3 hydrogen bond must be broken for C17 to loop out and expose the cleavage site to essential nucleotides in domain 1 (*17*).

The general role of metal ions in the cleavage reaction of the hammerhead ribozyme is also controversial. Initially, the pH dependence of the cleavage rate constant suggested that a metal hydroxide bound to the ribozyme acts as a general base in catalysis (*18*). Subsequently, the catalytic activity of the hammerhead ribozyme in the presence of monovalent cations alone was found to rule out an obligatory role of divalents (*19*−*21*). Cleavage kinetics in crystals indicate that the pH dependence arises from a metal-induced rate-limiting conformational change, rather than a chemical step (*22*). Most recently, Hampel and Burke have found, using hydroxyl radical footprinting, that the catalytic core becomes solvent-protected by folding at low millimolar Mg^{2+} concentrations. Their results support a model in which the ribozyme is folded into a crystal structure-like ground state at low Mg^{2+} concentrations, while only at higher Mg^{2+} concentrations does the catalytic transition state become accessible (*23*).

Clouet-d'Orval and Uhlenbeck have shown that the presence of an A·U tandem 3′ to the cleavage site in stem I accelerates catalysis 10-fold (*24*, *25*). This acceleration is primarily caused by a small increase in activation entropy, possibly due to the dynamic properties of the A·U tandem (*25*). To investigate the roles of metal ions, conformational changes, and this A·U tandem in the folding and function of the hammerhead ribozyme, we have carried out a comparative study between two constructs, HHL and HHα. Ribozyme HHL resembles a three-strand construct used by Lilley and co-workers to study the Mg^{2+} dependence of folding by steady-state FRET (*8*). Ribozyme HHα is similar to the higher-activity ribozyme described by Clouet-d'Orval and Uhlenbeck (*24*, *25*).

We have used cleavage assays as well as time-resolved FRET (tr-FRET) based on time-correlated single-photon counting to correlate catalytic activity with the stem I−stem II distance and flexibility of donor−acceptor fluorophore-labeled ribozymes. This technique has previously been successfully applied to other small catalytic RNAs such as the hairpin and HDV ribozymes (*26*−*28*). Our results show that at saturating Mg^{2+} concentrations, pH 8, and 25 °C, both ribozymes cleave at comparable rates (5−10 min^{-1}). However, ribozyme HHα binds Mg^{2+} with a 10-fold higher affinity, explaining the higher activity of this enzyme at millimolar Mg^{2+} concentrations. Careful analysis of the stem I−stem II distance dependence on Mg^{2+} shows that both ribozymes fold by what can be described as a two-step metal binding process. In contrast to a previous two-step metal-induced folding model (*8*, *29*), the first transition we observe, with apparent Mg^{2+} dissociation constants in the physiological range of ∼1 mM, brings stems I and II close together in a conformation that resembles the crystal structure. The second transition, a minor global structural rearrangement, coincides with activation of the ribozyme. Interestingly, the widths of the distance distributions show a higher flexibility for HHα than for HHL at all Mg^{2+} concentrations. Our results are consistent with the recent model of Hampel and Burke based on hydroxyl radical footprinting, which suggests that low metal ion concentrations fold the ribozyme into a stable ground-state tertiary structure that is similar to the crystallographic structures, while higher metal ion concentrations facilitate the conformational change that accesses the transition state for catalysis (*23*). Combining their results with ours, we propose that the role of diffusely bound Mg^{2+} ions at millimolar concentrations is to orient stems I and II of the hammerhead ribozyme in a way that increases the probability of formation of a catalytically active core.

MATERIALS AND METHODS

Preparation of RNA Oligonucleotides. RNA oligonucleotides were purchased with 2′-protection groups from the Howard Hughes Medical Institute Biopolymer/Keck Foundation Biotechnology Resource RNA Laboratory at the Yale University School of Medicine (New Haven, CT) and were deprotected as suggested by the manufacturer (http://info.med.yale.edu/wmkeck/). The following sequences were used: (i) HHL construct, ribozyme strands HHL1 (5′-F-AAC GAC CGC UCA CUG AUG AGG CCC ACU CGA A-T-3′) and HHL2 (5′-UUC GAG UGG GCC GAA ACG UAC UAC G-3′), substrate HHLS (5′-CGU AGU ACG UCU GAG CGG UCG UU-3′), nonligatable 5′ product analogue HHL5′P (5′-CGU AGU ACG UCp-3′), and 3′ product HHL3′P (5′-UGA GCG GUC GUU-3′); and (ii) HHα construct, ribozyme strand HHα1 (5′-F-AAC GCU ACU GAU GAG AUU C-T-3′), substrate HHαS (5′-GGA AUC GAA ACG CGA AAG CGU CUA GCG-3′), nonligatable 5′ product analogue HHα5′P (5′-GGA AUC GAA ACG CGA AAG CGU Cp-3′), and 3′ product HHα3′P (5′-UAG CGU U-3′). F stands for 5′-fluorescein, T for 3′-tetramethylrhodamine, and p for 3′-phosphate; to obtain chemically blocked, noncleavable substrate analogues for minimal interference with our structural studies, the underlined C17 nucleotide was modified with a 2′-methoxy group (yielding substrate analogue SmC17). Deprotected RNA was purified by denaturing 20% polyacrylamide, 8 M urea, gel electrophoresis; diffusion elution into 0.5 M NH_4OAc, 0.1% SDS,

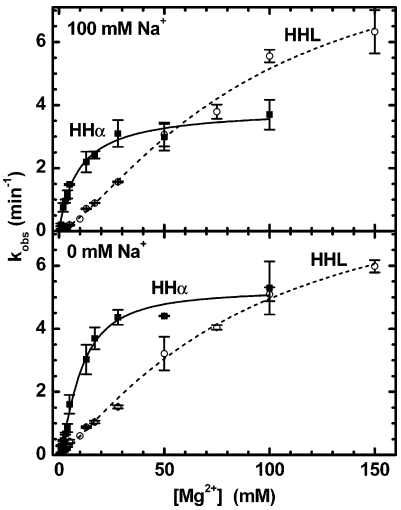

FIGURE 2: Mg^{2+} dependence of the observed cleavage rate constant for HHL (○) and HHα (■), under standard conditions (50 mM Tris-HCl, pH 8.0, and 25 °C), in the presence and absence of 100 mM NaCl, as indicated. The experimental data were fit to the cooperative binding equation (eq 1 in Materials and Methods): (- - -) HHL and (—) HHα. The fit parameters are given in Table 1.

and 0.1 mM EDTA overnight at 4 °C; chloroform extraction; ethanol precipitation; and C_8 reverse-phase HPLC with a linear acetonitrile gradient in triethylammonium acetate as previously described (*30*). 5′-Fluorescein was attached to the RNA by the manufacturer, while 3′-tetramethylrhodamine was incorporated postsynthetically as previously described (*30*, *31*). RNA concentrations were calculated from absorption at 260 nm and corrected for the additional absorption of fluorescein and tetramethylrhodamine by using the relations $A_{260}/A_{492} = 0.3$ and $A_{260}/A_{554} = 0.49$, respectively.

Cleavage Reactions. 5′-^{32}P-labeled substrates were prepared by phosphorylation with T4 polynucleotide kinase and [γ-^{32}P]ATP. All cleavage reactions were conducted under single-turnover (pre-steady-state) conditions. Standard buffer was 50 mM Tris-HCl (pH 8.0) either with or without 100 mM NaCl. Mg^{2+} concentrations were varied as shown in Figure 2. The ribozyme−substrate complex was preannealed in standard buffer by heating to 70 °C for 2 min and slow cooling over 5 min to room temperature. After preincubation for 15 min at 25 °C, an equal volume of standard buffer, supplemented with twice the required $MgCl_2$ concentration, was added to initiate the reaction. Final RNA concentrations were 1 μM each for strands HHL1 and HHL2, or 1 μM HHα1, and trace amounts (<1 nM) of the complementary 5′-^{32}P-labeled substrate. Reaction aliquots (2 μL) were taken at appropriate time intervals and the reactions quenched with 13 μL of stop solution (80% formamide, 0.025% xylene cyanol, 0.025% bromophenol blue, and 50 mM EDTA). For time points faster than 10 s, 1 μL of the preannealed ribozyme−substrate complex in standard buffer was placed in a microwell plate. The reaction was immediately initiated by addition of 1 μL of the desired salt solution, and quenched at the appropriate time with 13 μL of stop solution. The 5′-cleavage product was separated from the uncleaved substrate by denaturing 20% polyacrylamide, 8 M urea, gel electrophoresis, and was quantified and normalized to the sum of the substrate and product bands using a Storm 840 PhosphorImager with ImageQuant software (Molecular Dynamics). Error bars stem from at least two independent cleavage assays. Time traces of product formation were fit to the single-exponential first-order rate equation $y(t) = y_0 + A(1 - e^{-k_{obs}t})$, employing Marquardt−Levenberg nonlinear least-squares regression (Microcal Origin), where A is the final extent of cleavage and k_{obs} is the first-order rate constant. Mg^{2+} dependencies of this rate constant were fit to the binding equation

$$k_{obs} = k_{sat}\frac{[Mg^{2+}]^n}{[Mg^{2+}]^n + K_H{}^n} \quad (1)$$

to yield the cleavage rate constant k_{sat} under saturating Mg^{2+} conditions, the apparent metal ion dissociation constant K_H, and the cooperativity coefficient n (*32*).

Time-Resolved FRET Measurements. The global structure of the hammerhead ribozyme was studied as a function of Mg^{2+} concentration by tr-FRET analysis of ribozyme complexes doubly labeled with fluorescein and tetramethylrhodamine (Figure 1). The preannealed ribozyme−noncleavable substrate analogue or ribozyme−product complex (75 μL; either 1 μM HHL1 and 3 μM HHL2, to ensure saturation of the labeled HHL1 strand, or 1 μM HHα1; preannealed as described above with either 3 μM matching noncleavable substrate analogue or 5′- and 3′-product at 6 μM each) was incubated at either 25 or 4 °C for at least 15 min in standard buffer [50 mM Tris-HCl (pH 8.0) either with or without 100 mM NaCl], prior to collection of time-resolved emission profiles of the donor fluorescein using time-correlated single-photon counting similar to previously described procedures (*26*). A frequency-doubled Nd:YVO_4 laser (Spectra-Physics Millenia Xs-P, operated at 8.5 W) pumped a frequency-doubled, mode-locked Ti:sapphire laser (Spectra-Physics Tsunami, operated at 1 W) that excited fluorescein at 492 nm with pulses 2 ps in width, picked down to 4 MHz. Detection of isotropic emission to >40000 peak counts was performed under magic angle polarizer conditions at 520 nm (10 nm band-pass interference filter). Using a microchannel plate photomultiplier tube (Hamamatsu R3809U-50) feeding into a time-correlated single-photon counting card (SPC-630, Becker & Hickl), decays were collected in 4096 channels with a time increment of 12.20 ps/channel. An instrument response function was measured as the scattering signal from a dilute solution of nondairy coffee creamer to deconvolute the fluorescence decay data. To measure donor−acceptor distance distributions, two time-resolved fluorescence decays were collected, with and without the acceptor fluorophore. The fluorescein emission decay in the donor-only complex was used to extract the two or three intrinsic donor lifetimes τ_i, with their fractional contributions α_i, by a sum-of-exponentials fit. The data from the doubly labeled complex [$I_{DA}(t)$] were then fit with the Förster model for distance distributions

$$I_{DA}(t) = \sum_k f_k \int P_k(R) \sum_i \alpha_i \exp\left\{-\frac{t}{\tau_i}\left[1 + \left(\frac{R_0}{R}\right)^6\right]\right\} dR \quad (2)$$

where the first sum refers to the number of distributions, either one or two, each with fractional population f_k and

distance distribution $P_k(R)$. Distance distributions were modeled as weighted three-dimensional Gaussians

$$P_k(R) = 4\pi R^2 c \exp[-a(R-b)^2] \quad (3)$$

where a and b are parameters that describe the shape of the distribution and c is a normalization constant. Fitting was performed by nonlinear least-squares regression, with a, b, and f_k for each distribution as adjustable parameters. An additional adjustable parameter was a small fraction of singly labeled complex (always ≤10%), caused by photobleaching of the acceptor fluorophore during the titration experiment. The τ_i and α_i values from the donor-only decay were used under the assumption that each intrinsic donor lifetime is influenced independently by the presence of the acceptor at a distance R, and is split into a lifetime distribution by the distance distribution.

Mg^{2+} was titrated by incremental addition of 0.5 μL aliquots of appropriate $MgCl_2$ stock solutions in standard buffer, taking into account the volume change; the volume at the end of any given titration increased by not more than 12%. In all cases, except for the ribozyme−product complexes, a single distance distribution gave a good fit, as judged by the reduced χ^2 value (<1.3) and by evenly distributed residuals. To extract absolute distances, a value of 55 Å was used for the Förster distance, R_0, of fluorescein and tetramethylrhodamine (*26*), and a value of $^2/_3$ was assumed for the orientation factor, based on the high mobility of the fluorophores as evident from their low fluorescence anisotropies (0.15 for fluorescein and 0.1 for tetramethylrhodamine) (*30*, *31*).

The Mg^{2+}-induced folding of the hammerhead ribozyme can be interpreted in a simplified, general way as a two-step process in which metal ions are taken up by the Rz·S ribozyme−substrate complex with cooperativity coefficients m and n, following the reaction scheme

$$(Rz\cdot S)_N \overset{Mg^{2+}}{\rightleftharpoons} (Rz\cdot S)_L \overset{Mg^{2+}}{\rightleftharpoons} (Rz\cdot S^*)_H \quad (4)$$

where $(Rz\cdot S)_L$ is an intermediate yet inactive structure at low Mg^{2+} concentrations and $(Rz\cdot S^*)_H$ is the active structure at high Mg^{2+} concentrations. The associated, apparent metal ion dissociation constants K_L and K_H for these two equilibria are defined as

$$K_L{}^m = \frac{[(Rz\cdot S)_N][Mg^{2+}]^m}{[(Rz\cdot S)_L]} \quad K_H{}^n = \frac{[(Rz\cdot S)_L][Mg^{2+}]^n}{[(Rz\cdot S^*)_H]} \quad (5)$$

We assign to each conformer a characteristic mean distance between stems I and II such that the observed mean distance in solution, R_{obs}, is a weighted average of the species present in solution

$$\left.\begin{array}{l}(Rz\cdot S)_N \rightarrow R_N \\ (Rz\cdot S)_L \rightarrow R_L \\ (Rz\cdot S^*)_H \rightarrow R_H\end{array}\right\} \Rightarrow R_{obs} = \alpha_N R_N + \alpha_L R_L + \alpha_H R_H \quad (6)$$

where α_i values are defined as

$$\alpha_N = \frac{[(Rz\cdot S)_N]}{[(Rz\cdot S)_N] + [(Rz\cdot S)_L] + [(Rz\cdot S^*)_H]} = \frac{K_L{}^m K_H{}^n}{K_L{}^m K_H{}^n + K_H{}^n[Mg^{2+}]^m + [Mg^{2+}]^{m+n}}$$

$$\alpha_L = \frac{[(Rz\cdot S)_L]}{[(Rz\cdot S)_N] + [(Rz\cdot S)_L] + [(Rz\cdot S^*)_H]} = \frac{K_H{}^n[Mg^{2+}]^m}{K_L{}^m K_H{}^n + K_H{}^n[Mg^{2+}]^m + [Mg^{2+}]^{m+n}} \quad (7)$$

$$\alpha_H = \frac{[(Rz\cdot S^*)_H]}{[(Rz\cdot S)_N] + [(Rz\cdot S)_L] + [(Rz\cdot S^*)_H]} = \frac{[Mg^{2+}]^{m+n}}{K_L{}^m K_H{}^n + K_H{}^n[Mg^{2+}]^m + [Mg^{2+}]^{m+n}}$$

thus, R_{obs} can be expressed as a function of the Mg^{2+} concentration and dissociation constants

$$R_{obs} = \frac{K_L{}^m K_H{}^n R_N + K_H{}^n R_L[Mg^{2+}]^m + R_H[Mg^{2+}]^{m+n}}{K_L{}^m K_H{}^n + K_H{}^n[Mg^{2+}]^m + [Mg^{2+}]^{m+n}} \quad (8)$$

The stem I−stem II distance dependence on Mg^{2+} concentration was fit to eq 8, with the following fixed input parameters: R_N, the distance in the absence of Mg^{2+} as directly accessed by tr-FRET; and K_H and n, the dissociation constant and cooperativity coefficient, respectively, as directly measured in our cleavage assays (eq 1).

FRET Gel Mobility Assays. FRET gel mobility assays were conducted, as previously described (*27*), to test the homogeneity of ribozyme−substrate and −product complexes. Nondenaturing gel electrophoresis was performed in 20% polyacrylamide (19:1 acrylamide:bisacrylamide), 50 mM Tris-HOAc (pH 8), and 10 mM $Mg(OAc)_2$. Ten picomoles of doubly fluorophore-labeled strand HHα1 or 10 pmol of labeled HHL1 and 30 pmol of unlabeled HHL2 were annealed in 50 mM Tris-HOAc (pH 8), 10 mM $Mg(OAc)_2$, and 10% glycerol, by heating for 2 min to 70 °C and cooling to room temperature. The ribozyme was equilibrated at 25 °C for at least 15 min prior to addition of 30 pmol of substrate or noncleavable substrate analogue, or 60 pmol each of the 5′- and 3′-products (total volume of 10−20 μL). The electrophoresis unit was assembled and pre-equilibrated at 4 °C; the samples were loaded onto the gel, and an electric field of 6 V/cm was immediately applied. After electrophoresis for 15 h, the gel was scanned between its low-fluorescence glass plates in a FluorImager SI fluorescence scanner with ImageQuant software (Molecular Dynamics) as previously described (*27*, *33*). Briefly, a 488 nm laser excites fluorescein, and fluorescence is collected by a fiber optic bundle, to be quantified by a photomultiplier tube, after passing through either a 530 nm band-pass filter (donor fluorescein) or a 610 nm long-pass filter (acceptor tetramethylrhodamine). RNAs labeled with only fluorescein and only tetramethylrhodamine were included as color calibration standards. The relative FRET efficiency is calculated from the selected band intensities as $F_{acceptor}/F_{donor}$. With readout of F_{donor} defined as green and $F_{acceptor}$ as red, the correspond-

ing color images were superimposed using Photoshop 5.5 (Adobe) to generate Figure 6.

Generating Atomistic Models of Our Hammerhead Ribozyme Constructs. Structural models for ribozymes HHL and HHα based on the crystal structure [PDB entry 301D (*6*)] were generated using the program ERNA-3D (*34*). ERNA-3D was first used to produce initial models based on the primary and secondary structures of HHL and HHα. Next, the catalytic core structures of these initial models were adapted to the atomic coordinates of the crystal structure. Finally, stems I−III were interactively maneuvered until they fully aligned with those in the crystal structure. Similarly, models for ribozymes HHL and HHα based on the NMR structure were generated [coordinates graciously provided by A. Pardi (*35*)].

Electrostatic Potential Calculations. Structural coordinates of the hammerhead ribozyme crystal and NMR structures were obtained from the Protein Data Bank [PDB entry 301D (*6*)] and A. Pardi [personal communication (*35*)], respectively. Water molecules and metal ions observed crystallographically were not included in our calculations. Molecular surfaces were calculated using van der Waals atomic radii. The unit charge carried by the backbone phosphates was distributed equally between the two ionizable phosphate oxygens. Electrostatic potentials were calculated using the finite difference nonlinear Poisson−Boltzmann (NLPB) equation implemented in the program Delphi/Qnifft14 (*36*, *37*). Three-dimensional structures and electrostatic potentials were rendered using GRASP (*38*) to generate Figure 9.

RESULTS

HHα1 is a short-stemmed hammerhead ribozyme that was discovered by Clouet-d'Orval and Uhlenbeck (*24*). The authors found that an A·U tandem at the base of stem I, immediately 3′ of the cleavage site, causes a 10-fold acceleration of cleavage over other hammerhead ribozymes through a small increase in activation entropy, invoking the notion that dynamic properties of the A·U tandem may stimulate catalysis (*25*). To further investigate the effect of this sequence element on the folding and function of the hammerhead ribozyme, we performed a comparative study between two ribozymes, HHα and HHL. Ribozyme HHα is a fluorophore-labeled construct based on HHα1. Ribozyme HHL is similar to a construct previously used by Lilley and co-workers to characterize Mg^{2+}-induced folding by steady-state FRET (*8*, *29*). Given the Y-shaped global structure of the hammerhead ribozyme, we site-specifically labeled the two stems that come closest to each other, stems I and II, with fluorescein and tetramethylrhodamine, respectively, as a FRET pair. To avoid fluorophore quenching by adjacent guanines (*30*, *39*), especially of the donor fluorescein that is monitored by tr-FRET, two A·U base pairs each were added to the ends of stems I and II of ribozyme HHL and stem I of ribozyme HHα, yielding the constructs in Figure 1.

Cleavage Assays Show Different Mg^{2+} Dissociation Constants for HHL and HHα, with Maximum Cleavage at High, Nonphysiological Mg^{2+} Concentrations. We first compared the Mg^{2+} dependencies of the cleavage activities of HHα and HHL under single-turnover conditions at pH 8.0 and 25 °C, in the presence and absence of 100 mM NaCl (see Materials and Methods). Figure 2 shows the resulting first-order rate constants, k_{obs}, as a function of Mg^{2+} concentration. In the absence of Na^+, they increase from 0.05 to 5.1 min^{-1} and from 0.3 to 5.3 min^{-1} for HHL and HHα, respectively, between 1 and 100 mM Mg^{2+}. Addition of 100 mM NaCl slightly decreases the rate constants only at the lowest Mg^{2+} concentrations for HHL, but throughout the entire Mg^{2+} range for HHα (Figure 2). Significantly, the observed rates for ribozyme HHα begin to saturate at Mg^{2+} concentrations above 20 mM in both the absence and presence of NaCl, while HHL is still not fully saturated at the highest Mg^{2+} concentration of 150 mM. We fit all Mg^{2+} dependencies to the cooperative binding equation (eq 1), yielding the parameters listed in Table 1. Mg^{2+} binding shows little cooperativity ($n \approx 1$). The derived apparent dissociation constants, K_H, suggest that Mg^{2+} binds with an ∼9-fold higher affinity to HHα than to HHL, while the maximum rate reached at a saturating Mg^{2+} concentration, k_{sat}, is slightly higher for HHL. That is, although under standard hammerhead ribozyme assay conditions, up to 10 mM Mg^{2+}, HHα cleaves 3−5-fold faster than HHL, given sufficient Mg^{2+}, HHL can cleave at least as fast as HHα (Figure 2). In both cases, however, only high, nonphysiological Mg^{2+} concentrations can fully activate the ribozyme. In previous measurements with HHα at pH 6, an even higher apparent Mg^{2+} dissociation constant was found than in our measurements at pH 8, indicating a possible pH dependence of Mg^{2+} binding (*24*).

Table 1: Parameters Describing the Mg^{2+} Dependence of Cleavage Activity of Hammerhead Ribozymes HHL and HHα[a]

construct	[Na^+] (mM)	K_H (mM)	n	k_{sat} (min^{-1})
HHL	0	90 ± 17	1.2 ± 0.1	9 ± 1.0
	100	90 ± 21	1.4 ± 0.1	10 ± 1.4
HHα	0	10 ± 1.1	1.5 ± 0.1	5.2 ± 0.2
	100	10 ± 2.0	1.0 ± 0.1	3.9 ± 0.3

[a] The apparent Mg^{2+} binding constants K_H, associated cooperativity constants n, and cleavage rate constants k_{sat} at saturating Mg^{2+} concentrations were derived from the fits in Figure 2 as described in Materials and Methods (eq 1) under standard cleavage conditions: single turnover, 50 mM Tris-HCl, pH 8.0, either with or without 100 mM NaCl, as indicated, and 25 °C. Errors are one standard deviation as determined by the fit.

Time-Resolved FRET Titrations Suggest a Major, Low-Mg^{2+} Concentration Folding Transition and a Minor, High-Mg^{2+} Concentration, Catalytically Activating Transition. Steady-state fluorescence spectroscopy has been previously used to determine the mean FRET efficiency of fluorophore-labeled hammerhead ribozymes (*7*, *8*). These steady-state experiments, however, can only provide qualitative information about the fluorophore distances, whereas a technique such as time-resolved FRET (tr-FRET) yields quantitative distances between the donor and acceptor fluorophores (*28*, *30*). Furthermore, tr-FRET determines the distribution of distances between the fluorophore pair. The mean of such a distribution relates to the single FRET efficiency measured in steady-state experiments, while the width is a unique observation in time-resolved measurements and arises in part from the intrinsic flexibility of the RNA in solution (*30*).

We have used the capabilities of tr-FRET to address three specific questions. (i) At what Mg^{2+} concentrations do stems I and II reach a distance comparable to the crystallographically observed one? (ii) How significant is the structural change that activates the hammerhead ribozyme at high Mg^{2+}

Table 2: Parameters Describing the Mg^{2+} Dependence of Global Folding of Hammerhead Ribozymes HHL and HHα As Monitored by tr-FRET[a]

construct	T (°C)	[Na^+] (mM)	R_N (Å)	K_L (mM)	m	R_L (Å)	K_H (mM)	n	R_H (Å)
HHL	25	0	77.3 ± 0.4	0.78 ± 0.03	1.1 ± 0.03	65.6 ± 0.2	90	1.2	61.8 ± 0.9
		100	72.6 ± 0.1	2.7 ± 0.2	1.2 ± 0.04	65.8 ± 0.2	90	1.4	63.0 ± 0.9
	4	0	77.0 ± 0.4	0.60 ± 0.04	1.1 ± 0.1	59.4 ± 0.6	90	1.2	62 ± 4
		100	68.6 ± 0.4	4.5 ± 0.9	1.1 ± 0.1	59 ± 1	90	1.4	62 ± 4
HHα	25	0	ND	ND	ND	ND	10	1.5	ND
		100	54.4 ± 0.1	1.7 ± 0.5	1.2 ± 0.1	50.5 ± 0.7	10	1.0	46.2 ± 0.3
	4	0	54.5 ± 0.3	0.16 ± 0.01	1.3 ± 0.1	41.2 ± 0.2	10	1.5	42.9 ± 0.2
		100	48.2 ± 0.6	6 ± 2	0.8 ± 0.1	39 ± 1	10	1.0	46.0 ± 0.5

[a] The apparent Mg^{2+} binding constants K_L, associated cooperativity constants m, and mean distances R_L and R_H were derived from the fits in Figure 4 as described in Materials and Methods (eq 8) under standard cleavage conditions: single turnover, 50 mM Tris-HCl, pH 8.0, either with or without 100 mM NaCl, and at either 25 or 4 °C, as indicated. R_N, the distance in the absence of Mg^{2+}, was taken directly from the "no-Mg^{2+}" tr-FRET measurement, and K_H and n, the dissociation constant and cooperativity coefficient of catalytic activation, respectively, were derived from our cleavage assays (Table 1). Errors are one standard deviation as determined by the fit, or, in the case of R_N, derived from at least duplicates of the no-Mg^{2+} measurement.

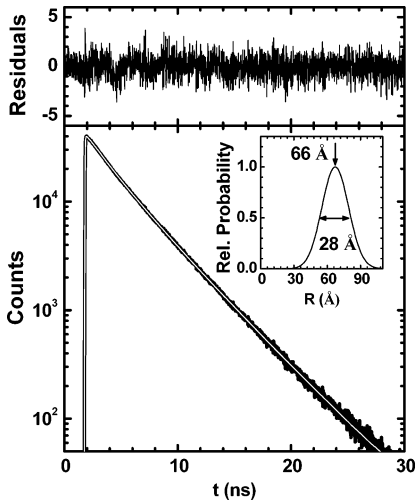

FIGURE 3: HHL donor fluorescence decay in the presence of the acceptor fluorophore, in 50 mM Tris-HCl (pH 8.0), 9 mM $MgCl_2$, and 100 mM NaCl at 25 °C. The bottom panel shows the experimental fluorescence decay (black line) and the corresponding fit (white line) to eq 2 (Materials and Methods), which converged to a reduced χ^2 value of 1.1. The top panel shows fit residuals. The inset shows the resulting single-distance distribution, yielding a mean distance of 66 Å and a fwhm of 28 Å.

concentrations? (iii) Does HHα, with its stimulated cleavage activity due to an A·U tandem 3′ to the cleavage site, exhibit enhanced global flexibility?

To this end, we have quantified and compared the Mg^{2+}-dependent global conformational changes of hammerhead ribozymes HHL and HHα in their noncleavable substrate analogue complexes (with a 2′-methoxy group at the cleavage site to preserve folding but block chemistry; see Materials and Methods). Figure 3 shows, as an example, the donor fluorescence decay curve of fluorescein-tetramethylrhodamine-labeled HHL at 9 mM Mg^{2+} and 25 °C in the absence of Na^+. This decay curve, as well as all other measurements of the substrate complexes of both HHL and HHα, fit to a single donor−acceptor distance distribution with an excellent reduced χ^2 of <1.3 and no systematic deviation in residuals, and in all cases, the inclusion of a second distance distribution did not improve the fit.

Panels A and B of Figure 4 give the mean stem I−stem II distances derived by tr-FRET for HHL and HHα, respectively, in standard buffer as a function of Mg^{2+} concentration at 25 and 4 °C, and in the presence and absence of 100 mM NaCl, as indicated. With increasing Mg^{2+} concentrations, the end-to-end distance of stems I and II decreases substantially, as expected for their approach into a Y-shaped global structure (the only exception is HHα at 25 °C in the absence of Na^+, which possibly is due to incomplete substrate binding; see below). Increasing the Mg^{2+} concentration to 150 mM decreases the final stem I−stem II distance by less than 2 Å (data not shown). Thus, the only large conformational change occurs at low millimolar concentrations, and is close to completion at 10 mM Mg^{2+}, far below full catalytic activation of the ribozyme (compare Figures 2 and 4). To quantify the changes at low and high Mg^{2+} concentrations, we fit the Mg^{2+} dependence of the mean stem I−stem II distance to the binding model in eq 8 (Materials and Methods). This binding model, based on eq 4, assumes that the mean stem I−stem II distances observed by tr-FRET are inherently ensemble-averaged over three conformational species: (i) the initial Mg^{2+}-free ribozyme−substrate complex $(Rz{\cdot}S)_N$ with a mean stem I−stem II distance R_N, (ii) the folding intermediate $(Rz{\cdot}S)_L$ with a substantially decreased stem I−stem II distance R_L, which is induced by Mg^{2+} binding at a comparably low (millimolar) bulk concentration (apparent dissociation constant K_L), and (iii) the fully cleavage-activated hammerhead ribozyme conformer $(Rz{\cdot}S^*)_H$ with a mean stem I−stem II distance R_H, which forms only at high (tens of millimolar) bulk Mg^{2+} concentrations (apparent dissociation constant K_H). Additional conformational species may be proposed, but three is the minimal number required to fully explain both our tr-FRET and cleavage data. From our cleavage assays, we have independently measured the values of K_H and its associated cooperativity constant, n, which characterize the Mg^{2+}-induced folding event that leads to catalytic activation of the hammerhead ribozyme. Additionally, we directly obtain R_N, the mean stem I−stem II distance in the absence of Mg^{2+}, from our tr-FRET measurements. By holding K_H, n, and R_N fixed, we can accurately determine the remaining parameters in eq 8 (Table 2).

The fit results in Table 2 quantify the observation from Figure 4. Ribozyme HHL undergoes its major conformational change at low Mg^{2+} concentrations. The associated apparent Mg^{2+} binding constants K_L for HHL in the absence of Na^+ are 0.75 and 0.5 mM at 25 and 4 °C, respectively, and the mean stem I−stem II distance decreases from 77 (R_N) to 66 Å (R_L) and from 77 (R_N) to 59 Å (R_L), respectively. Lowering

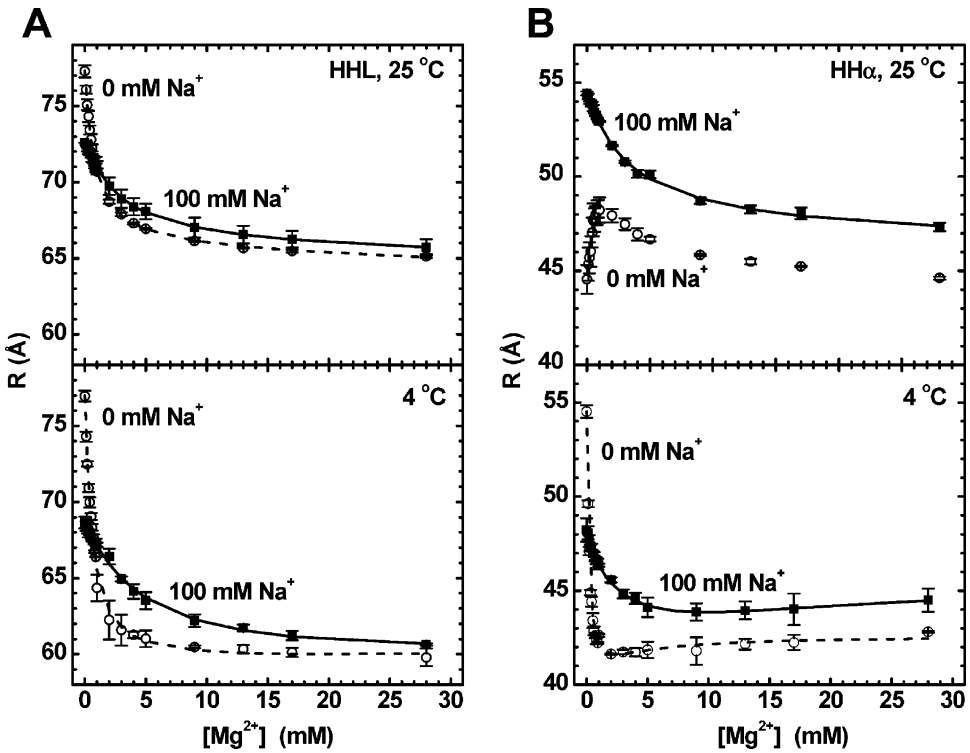

FIGURE 4: Average stem I−stem II distance of ribozymes HHL (A) and HHα (B) as a function of Mg^{2+} concentration under standard buffer conditions (50 mM Tris-HCl and pH 8.0) in the presence (■) and absence (○) of 100 mM NaCl, at 4 and 25 °C, as indicated. The experimental data were fit to eq 8 of the Mg^{2+} binding model (Materials and Methods; solid and dashed lines), and the resulting fit parameters are given in Table 2.

the temperature from 25 to 4 °C decreases the mean stem I−stem II distance R_L of the $(Rz{\cdot}S)_L$ species, possibly due to a more tightly folded RNA at the lower temperature. Addition of 100 mM Na^+ has two main consequences, at both 25 and 4 °C. (i) The Mg^{2+} concentration necessary to induce this initial conformational change increases (specifically, K_L increases by factors of ∼4 and ∼10 at 25 and 4 °C, respectively), consistent with competition of Mg^{2+} with Na^+ for binding to the RNA at these low Mg^{2+} concentrations. (ii) The mean stem I−stem II distance in the initial Mg^{2+}-free state, R_N, decreases, suggesting that Na^+ begins to prefold stems I and II into a more acute angle, although Mg^{2+} does this more efficiently. The cooperativity constant, *m*, of this major conformational change is generally close to 1 (Table 2), indicating that metal ions bind largely noncooperatively under all conditions that were tested.

The second transition occurs at higher Mg^{2+} concentrations, coinciding with the activation of HHL. During this comparably minor transition, the mean stem I−stem II distance at 25 °C decreases only slightly from 66 (R_L) to 62 Å (R_H) and from 66 (R_L) to 63 Å (R_H) in the absence and presence of 100 mM Na^+, respectively, while at 4 °C, it increases slightly from 59 (R_L) to 62 Å (R_H), in both the absence and presence of 100 mM Na^+. Generally, the addition of Na^+ does not have a significant effect on the observed distances; similarly, Na^+ did not affect the apparent Mg^{2+} dissociation constant K_H in the cleavage assays (Table 1). This observation is consistent with the idea that 100 mM monovalent Na^+ does not effectively compete with a similar concentration of the divalent Mg^{2+}.

Likewise, Figure 4B and Table 2 show that HHα undergoes two conformational transitions, although the measured mean stem I−stem II distances are shorter than for HHL, as expected for a construct with considerably shorter stems (Figure 1). In particular, HHα undergoes its major conformational change at low Mg^{2+} concentrations, with apparent Mg^{2+} binding constants K_L of 1.7 mM (25 °C, no Na^+), 0.16 mM (4 °C, no Na^+), and 6 mM (4 °C, 100 mM Na^+); the associated mean stem I−stem II distance decreases are from 54 (R_N) to 51 Å (R_L), from 55 (R_N) to 41 Å (R_L), and from 48 (R_N) to 39 Å (R_N), respectively (Table 2). Again, lowering the temperature from 25 to 4 °C decreases the mean stem I−stem II distance R_L of the $(Rz{\cdot}S)_L$ species. Addition of 100 mM Na^+ substantially increases the Mg^{2+} concentration necessary to induce this initial conformational change, while the mean stem I−stem II distance in the initial Mg^{2+}-free state, R_N, decreases in the presence of Na^+. The cooperativity constants, *m*, for this major conformational change are again generally close to 1 (Table 2).

The conformational transition that activates hammerhead ribozyme HHα at higher Mg^{2+} concentrations is more pronounced than for HHL. The mean stem I−stem II distance at 25 °C decreases from 51 (R_L) to 46 Å (R_H) in the presence of 100 mM Na^+, while at 4 °C, it increases from 41 (R_L) to 43 Å (R_H) and from 39 (R_L) to 46 Å (R_H) in the absence and presence of 100 mM Na^+, respectively. The latter values suggest that the addition of Na^+ may have a more significant effect on the activating conformational change of HHα than on that of HHL. Only the Mg^{2+} titration of HHα at 25 °C and in the absence of Na^+ behaves considerably differently. It shows an initial increase in the mean stem I−stem II distance between 0 and 1 mM Mg^{2+}, followed by a decrease above 1 mM (Figure 4B). Since this behavior is not reproduced at 4 °C (Figure 4B), we cannot rule out the possibility that at a low ionic strength and an elevated temperature the substrate does not fully saturate ribozyme

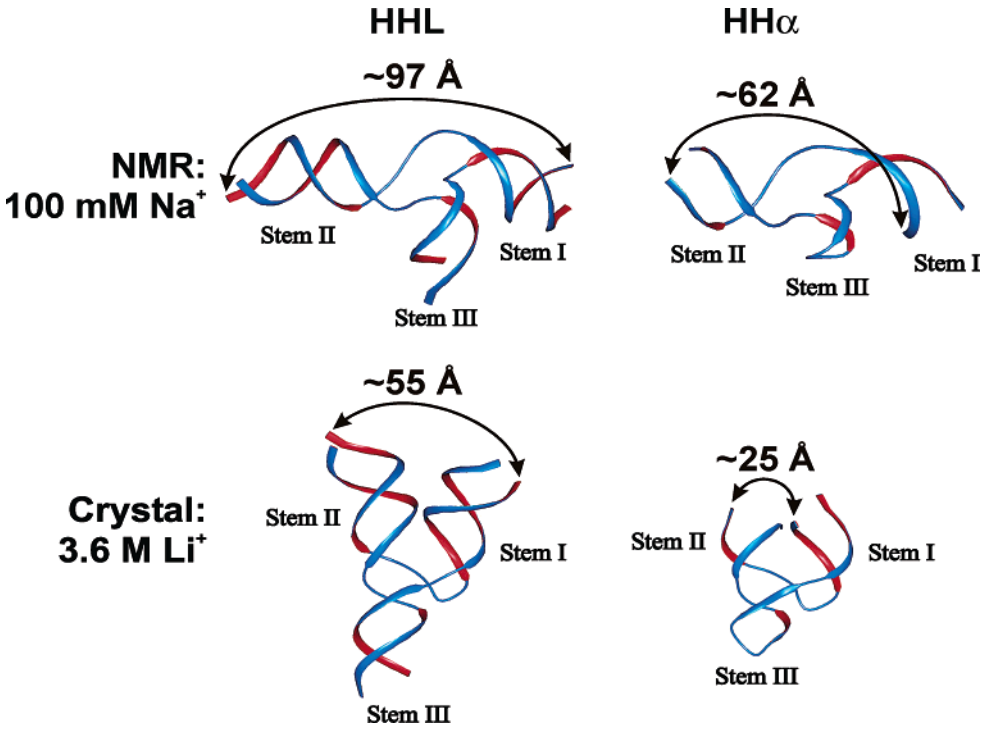

FIGURE 5: Ribbon representation of the atomistic model structures of ribozymes HHL (left) and HHα (right), based on the crystal structure (bottom panels) (*6*) and the NMR structure (top panels) (A. Pardi, personal communication). The distance between the 5′ end of stem I and the 3′ end of stem II was measured for comparison with our tr-FRET data.

HHα due to the relatively short stems that mediate substrate binding (Figure 1). Therefore, we have abstained from interpreting this particular Mg^{2+} titration in more detail.

Distance Measurements Are Consistent with Models Based on the Crystal Structure, but Not the NMR Structure. We have generated atomistic models of our hammerhead ribozyme constructs HHL and HHα based on the crystal structure determined in 3.6 M Li^+ [PDB entry 301D (*6*)], as well as the NMR structure determined in 100 mM Na^+ [coordinates kindly provided by A. Pardi (*35*)], employing the modeling tools of the program ERNA-3D (*34*) (see Materials and Methods). We then measured the distances between the 5′ end of stem I and the 3′ end of stem II, where the two fluorophores are attached. The resulting values can be compared with the experimental values derived from tr-FRET (Figure 5) to determine the Mg^{2+} concentrations at which stems I and II reach a distance comparable to the one observed in the crystal structure. In our experiments, however, we expect to measure average values that are 0−15 Å longer than those of the model, due to the presence of two fluorophore attachment linkers [the additional distance varies with the direction of projection away from the RNA (*7*)]. Indeed, the distances between the fluorophore attachment sites in our models based on the crystal structure [55 and 25 Å for HHL and HHα, respectively (Figure 5)] are systematically shorter than those measured in our experiments [60−65 Å for HHL and 40−45 Å for HHα (Figure 4)]. That is, even after the first, low-Mg^{2+} concentration, conformational transition, both of our hammerhead ribozymes are in a global structure consistent with the crystallographically observed one. In contrast, the distances between the fluorophore attachment sites in our models based on the NMR structure are longer [97 and 62 Å for HHL and HHα, respectively (Figure 5)] than the tr-FRET distances [R_N = 73 and 54 Å for HHL and HHα, respectively (Table 2)] under conditions similar to those in the NMR experiment (0 mM Mg^{2+}, 100 mM Na^+, and 25 °C). Thus, the tr-FRET measurements are not consistent with the NMR structure, since correcting for the linker length would further decrease the tr-FRET distances. This discrepancy is perhaps not surprising since the exact conformation of the catalytic core could not be determined in the NMR experiments (*35*), and may be much more compact than in our model. In addition or alternatively, differences in the pH (5.5 in the NMR and 8.0 in our tr-FRET studies) or RNA concentration (600−1900 μM in the NMR and 1 μM in our tr-FRET studies) or the presence of filamentous phage at 15−30 mg/mL in the NMR experiment may explain this discrepancy.

It should be pointed out that while the major conformational change at low, close-to-physiological, Mg^{2+} concentrations (K_L between 0.2 and 6 mM) already aligns stems I and II in a geometry similar to the crystal structure obtained in 3.6 M Li^+, only high, nonphysiological Mg^{2+} concentrations (K_H between 10 and 90 mM) fully activate both of our hammerhead ribozymes with a minor global structural rearrangement. HHL and HHα behave similarly in this regard, except that the Mg^{2+} requirements for the activation of HHα are 9-fold lower.

HHα Shows Increased Stem I−Stem II Flexibility. Figure 6 shows the full width at half-maximum (fwhm) of the fluorophore distance distributions from our tr-FRET analysis as a function of Mg^{2+} concentration (4 °C and no Na^+; other conditions gave similar results). Analysis of the fwhm enables us to address whether HHα (with its enhanced cleavage activity due to an A·U tandem 3′ to the cleavage site) exhibits enhanced global flexibility. Both HHL and HHα show a substantial fwhm, but that of HHα is larger over the entire Mg^{2+} concentration range. This is significant given that stems I and II are shorter in HHα than in HHL by 5 and 8 bp (~14 and ~22 Å), respectively (Figure 1).

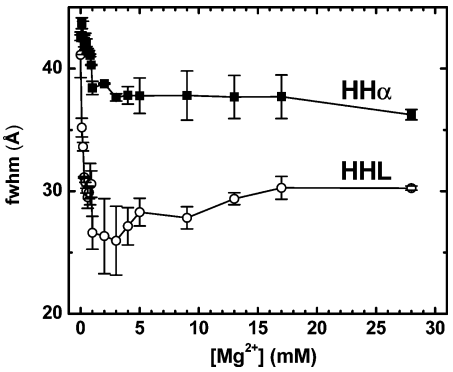

FIGURE 6: Mg^{2+} dependence of the full width at half-maximum (fwhm) of the measured distance distributions for HHL (○) and HHα (■) in 50 mM Tris-HCl (pH 8.0) and 100 mM NaCl at 25 °C.

Interestingly, during the initial low-Mg^{2+} concentration folding step, the fwhm of both constructs decreases; that is, Mg^{2+} somewhat restricts conformational space. The addition of 100 mM Na^+ dampens these changes in the fwhm and relative flexibility for both constructs (data not shown), again suggesting that Na^+ competes with Mg^{2+} during the initial, low-Mg^{2+} concentration conformational change.

Two factors can contribute to the fwhm values of the fluorophore distance distributions measured by tr-FRET: the intrinsic dynamics of the distance between the attachment sites of the fluorophores and the mobility of the fluorophores themselves at the end of their attachment linkers. However, the fact that in our direct comparison of the HHL and HHα constructs significant differences in the fwhm are observed, while the fluorophores and their attachment linkers are identical, suggests that our observations indeed provide evidence for differences in ribozyme flexibility. Specifically, they are consistent with the notion that hammerhead ribozyme HHα is characterized by enhanced global flexibility between its stems I and II, in agreement with the previously observed beneficial increase in activation entropy (*24*, *25*).

The Ribozyme−Product Complex Shows a Bimodal Distance Distribution. Blount and Uhlenbeck (*40*) have invoked a conformational equilibrium following cleavage to explain the observed enhanced ligation of a cross-linked hammerhead ribozyme−product complex. Their results suggest that chemical cross-linking of stems I and II of the hammerhead ribozyme constrains the product complex into an intermediate structure that more closely resembles the transition state, thereby increasing the reverse ligation rate relative to a non-cross-linked ribozyme. However, no direct structural evidence for such an intermediate has been presented. We have searched for such an intermediate by tr-FRET, characterizing the stem I−stem II distance distributions of ribozyme−product analogue complexes of constructs HHL and HHα in standard buffer at 10 mM Mg^{2+} and 25 °C in the presence and absence of 100 mM Na^+ (all conditions gave similar results). In these product analogue complexes, the 5′ product contains a 3′ phosphate that conserves the negative charge in the active site while blocking ligation, which requires a 2′,3′-cyclic phosphate instead. In contrast to the ribozyme−substrate complex (Figure 3), the donor lifetime distributions of both product complexes are fit considerably better with bimodal Gaussian distance distributions ($\chi^2 = 1.1$; Figure 7) than with a single distribution ($\chi^2 = 1.4$; Figure 7). HHL

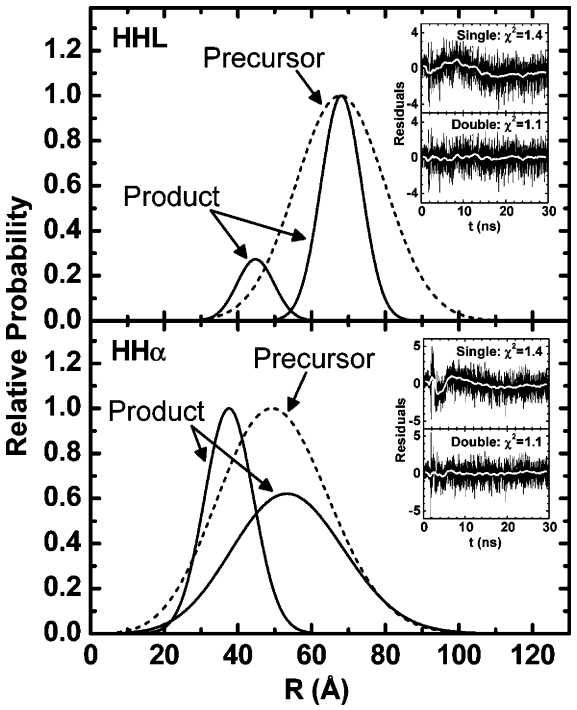

FIGURE 7: Bimodal distance distributions of 1 μM HHL (top panel) and 1 μM HHα (bottom panel) in complex with each of their corresponding 5′ and 3′ products (6 μM) in 50 mM Tris-HCl (pH 8.0), 9 mM Mg^{2+}, and 100 mM NaCl at 25 °C. The resulting parameters are as follows: (top) $R_{obs}(1) = 44$ Å, fwhm(1) = 12 Å, and population(1) = 21% and $R_{obs}(2) = 66$ Å, fwhm(2) = 13 Å, and population(2) = 79% and (bottom) $R_{obs}(1) = 37$ Å, fwhm(1) = 15 Å, and population(1) = 65% and $R_{obs}(2) = 53$ Å, fwhm(2) = 30 Å, and population(2) = 35%. Insets show fit residuals (black lines) using a single and a double distribution, as indicated, and their running average over 100 data points (white lines), showing that the double distribution gives more randomly distributed residuals as well as lower χ^2 values in both cases. Dashed lines are single distance distributions measured for the noncleavable substrate analogue complexes under identical conditions, showing that the longer distance product complex distributions correspond to the noncleavable distributions.

has 79% of its product complex population centered around a mean stem I−stem II distance of 66 Å (fwhm = 12 Å) and 21% around 44 Å (fwhm = 12 Å) (Figure 7), while HHα has 35% of its product complex population centered around a mean distance of 53 Å (fwhm = 30 Å) and 65% around 37 Å (fwhm = 16 Å) (Figure 7; the HHα distributions are perhaps less well defined because of their substantial overlap). Significantly, both ribozymes show a second distance distribution that has a shorter stem I−stem II distance than that observed for the respective ribozyme−substrate complexes under similar conditions (25 °C, 9 mM Mg^{2+}, and 100 mM Na^+; dashed lines in Figure 4). One of these distance distributions may be the intermediate structure that forms immediately after substrate cleavage and structurally still resembles the transition state as proposed in the mechanistic model by Blount and Uhlenbeck (*40*).

A FRET Gel Mobility Assay Demonstrates the Homogeneity of Our Ribozyme Complexes. We have previously developed a gel mobility assay that measures the relative FRET efficiencies of donor−acceptor fluorophore-labeled RNA complexes after electrophoresis in nondenaturing polyacrylamide gels, thus testing their conformational homogeneity (*27*, *41*). Figure 8 shows such gel mobility assays, performed at pH 8, 10 mM Mg^{2+}, and 4 °C (see Materials

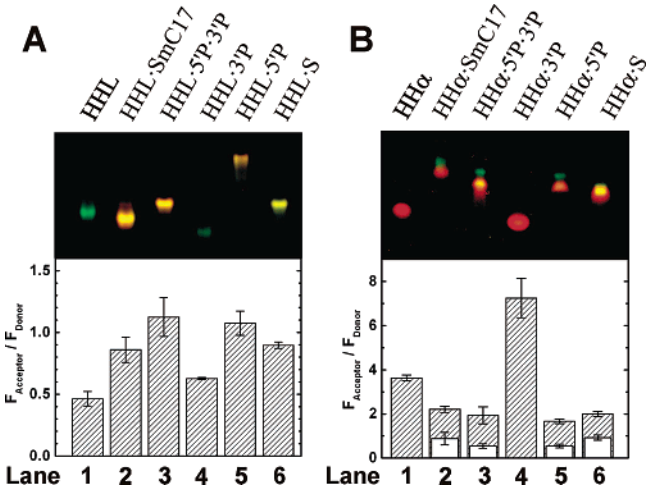

FIGURE 8: Nondenaturing gel electrophoresis of various HHL (A) and HHα (B) complexes as indicated above each lane (Materials and Methods). Donor emission is represented as green and acceptor emission as red. The bottom panels are corresponding FRET ratios. White bars indicate FRET ratios of secondary bands with lower gel mobility.

and Methods), and their FRET quantification for ribozymes HHL and HHα alone and in complex with their noncleavable substrate analogues (SmC17), their 5′ and 3′ products (5′P and 3′P, respectively), and their cleavable substrates (S). All complexes of HHL migrate as single bands (Figure 8A). The free ribozyme (lane 1) shows a "green-shifted" band with a low FRET ratio (acceptor:donor fluorescence). The binding of a noncleavable substrate analogue (lane 2) increases the FRET ratio, consistent with the folding of the complex into a Y shape with stems I and II in proximity of each other, as observed in our tr-FRET experiments. The ribozyme−product analogue complex (lane 3) has lower gel mobility and has a higher FRET ratio still; clearly, there are structural differences between the substrate and product analogue complexes, although on the time scale of gel migration we do not resolve two product complex conformers as we do by tr-FRET. Lanes 4 and 5, as controls, show that the ribozyme in complex with only the 3′ or 5′ product has very distinct gel mobility and FRET ratios. Finally, lane 6, loaded with the catalytically competent ribozyme−substrate complex, shows a band that comigrates with the product (lane 3) rather than the substrate analogue complex (lane 2), suggesting that the substrate indeed is cleaved in the nondenaturing gel (*27*). Interestingly, the FRET ratio of the authentic ribozyme−product complex is closer to that of the ribozyme−noncleavable substrate analogue, perhaps due to the fact that the ligatable 2′,3′-cyclic phosphate of this complex allows a cleavage ligation equilibrium to be established.

The HHα complexes in Figure 8B have FRET ratios consistently higher than those of HHL, as expected from a ribozyme with shorter stems (see structural models in Figure 5). The free ribozyme (lane 1), which in the absence of the substrate strand does not have any base-paired regions (Figure 1), has a very high FRET ratio, consistent with it being a random coil. Upon formation of the noncleavable substrate analogue complex (lane 2), the ribozyme is shifted into a major band with a lower gel mobility and a lower FRET ratio, indicative of the expected structure with a larger hydrodynamic radius and more helical structure, respectively. In addition, a second minor band (~20% of the major one), with an even lower gel mobility and FRET ratio, appears. The considerably lower FRET ratio of this secondary conformer indicates that the two fluorophores are further apart than in the major conformer. Interestingly, a similar band is observed in the ribozyme−product complex (both with product analogue and cleaved substrate, lanes 3 and 6, respectively) and the ribozyme−5′ product (lane 5) but not the ribozyme−3′ product complex (lane 4). Therefore, the presence of this band depends on the long sequence 5′ to the cleavage site, rather than the shorter sequence 3′ to the cleavage site (Figure 1). We did not find any evidence for such a defined secondary conformer in our tr-FRET analysis of the HHα ribozyme−noncleavable substrate complex, where a single distance distribution at 9 mM Mg^{2+} gave an excellent χ^2 value of 1.1 and no systematic deviation in residuals. The inclusion of a second distance distribution did not improve the fit, similar to our HHL analysis (Figure 3). It is possible that the sieving and caging effects of the polyacrylamide gel matrix or the low temperature (4 °C) during electrophoresis either slow the interconversion of existing conformers of the HHα hammerhead ribozyme or induce novel RNA conformations that are resolved as separate bands.

DISCUSSION

Biological catalysis is critically dependent on the proper juxtaposition of functional groups from substrate and enzyme to increase their local concentration and lower the entropic cost of the interaction (*42*). In the case of the hammerhead ribozyme, much controversy has resulted from the discovery that the active site shown in the crystal structure does not match the proposed mechanism. The substrate's regular A-type backbone geometry around C17, as observed in the crystal structure, does not seem to allow for the distorted in-line attack configuration at the scissile phosphate that is necessary for cleavage (*13*−*16*). One explanation may be that hammerhead ribozyme crystals are typically grown at high, nonphysiological cation concentrations (3.6 M Li^+) (*5*, *6*) where stems I and II are held in a potentially nonfunctional structure by intermolecular crystal contacts, due to head-to-head stacking of two molecules in the crystallographic unit cell. Recent evidence, however, suggests that crystal packing still allows for a local conformational change in which C17 loops out, thus exposing the scissile phosphate to the catalytic pocket of G5 and A6 in domain 1, which in turn leads to cleavage (*17*, *22*). The idea of a localized conformational change, however, contradicts the model proposed by Herschlag and co-workers in which a metal ion bridges the phosphates of A9 and the cleavage site in the transition state (*14*). To better understand folding and function in solution, we have exploited tr-FRET, in combination with cleavage assays, to quantify the extent and functional relevance of Mg^{2+}-induced changes in the stem I−stem II distance distribution of two hammerhead ribozyme variants, HHL and HHα.

Our results show that both ribozymes fold in a two-step metal-binding process. The first transition, with apparent Mg^{2+} dissociation constants in the physiological range (~1 mM), brings stems I and II close together in a conformation that resembles the crystal structure. The second, globally minor, structural adjustment coincides with activation of the

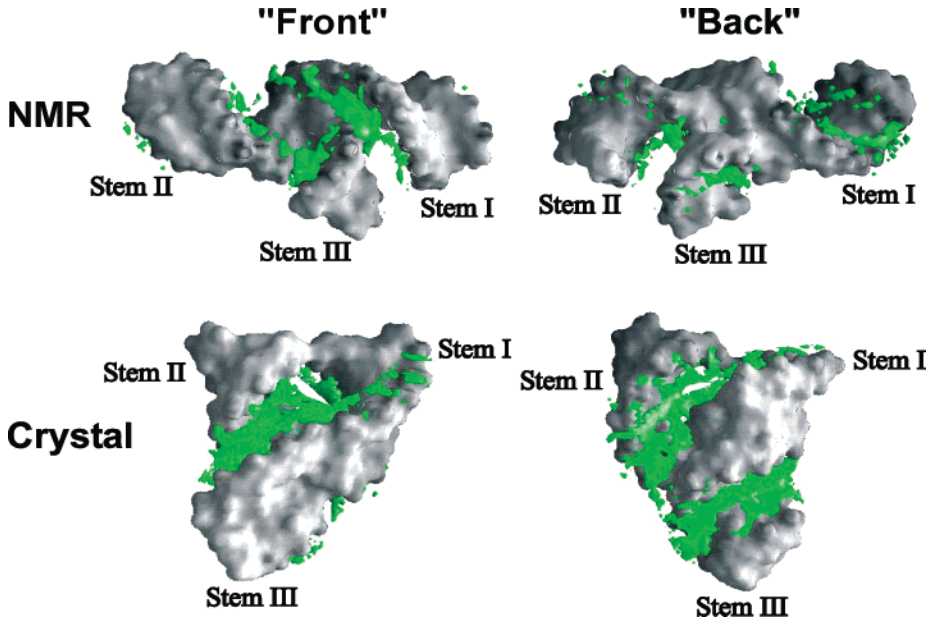

FIGURE 9: Three-dimensional 2.5 M Mg^{2+} isoconcentration contour maps (green) around the hammerhead ribozyme in its crystal and NMR structures, as calculated using the nonlinear Poisson−Boltzmann (NLPB) equation. Panels on the right are rotated 180° to show the "back" of the ribozyme. Calculations were carried out for bulk concentrations of 10 mM Mg^{2+} and 100 mM Na^{+}. More Mg^{2+} ions accumulate in the compact crystal structure, especially around the center of the junction and in the minor grooves.

ribozyme at high Mg^{2+} concentrations (90 mM for HHL and 10 mM for HHα). Our data are therefore largely consistent with the notions, suggested first by X-ray crystallography, that the functionally relevant conformation has stems I and II at an acute angle and that only a relatively small conformational change is required to reach the catalytic transition state (*5*, *17*, *22*, *43*). Additionally, we note that throughout the entire Mg^{2+} range, HHα has a more flexible stem I−stem II distance than HHL (Figure 6), an observation that may relate to its higher catalytic activity, consistent with the activation entropy increase previously reported (*25*).

Our observations are in agreement with other solution-based structural studies of the hammerhead ribozyme, particularly with recent hydroxyl radical footprinting data which suggest that millimolar Mg^{2+} concentrations induce formation of a solvent-protected catalytic core around nucleotides G5, A6, U7, G8, and A9 of the ribozyme and C17 of the substrate (*23*). As in the study presented here, it was noted that the ribozyme folds into the protected tertiary structure at Mg^{2+} concentrations significantly lower than those required for cleavage. It is now apparent that the solvent protection detected by hydroxyl radical footprinting at millimolar Mg^{2+} concentrations coincides with our first Mg^{2+}-induced transition, which brings stems I and II into a conformation resembling the crystal structure. While hydroxyl radical footprinting could not determine whether a large- or small-scale conformational change is required for catalysis (*23*), our tr-FRET results suggest that the required global structural change is relatively minor, in terms of the stem I−stem II distance.

Earlier solution studies of the hammerhead ribozyme have used steady-state FRET to measure the efficiency of a single energy transfer between two fluorophores attached to stems I and II (*7*, *8*, *29*). This energy transfer efficiency is related to the mean stem I−stem II distance derived from our tr-FRET measurements. Lilley and co-workers have previously employed steady-state FRET to characterize two consecutive Mg^{2+}-induced folding events of a hammerhead ribozyme very similar to our HHL construct (*8*, *29*). It is important to note, however, that we do not observe the same two transitions. The folding event at "low" Mg^{2+} concentrations observed by Lilley and co-workers, with an apparent Mg^{2+} dissociation constant of 0.1 mM, occurs at a Mg^{2+} concentration lower than our first transition, while their "high"-Mg^{2+} concentration event has an Mg^{2+} dissociation constant of 0.9 mM (*8*), comparable to our K_L of 0.6 mM under similar conditions [HHL, 4 °C, and no Na^{+} (Table 2)]. That is, the second transition, at millimolar Mg^{2+} concentrations, observed by Lilley and co-workers corresponds to the first transition observed in our work. It should be noted that our findings are not inconsistent with those of Lilley and co-workers, since the conformational change at sub-millimolar Mg^{2+} concentrations does not manifest itself in a stem I−stem II distance change, but only in distance changes involving stem III (*8*). In contrast to previous conclusions (*8*, *29*), our work shows that the large-scale conformational change is not catalytically activating, and a second, minor conformational adjustment is necessary to form the active state.

We have found the Mg^{2+} concentration required for catalytic activity to be nonphysiologically high (90 or 10 mM). At this high Mg^{2+} concentration, one can expect the polyanionic RNA backbone to become saturated with low-affinity, diffusely bound metal cations in addition to higher-affinity, site-bound metals (*44*, *45*). In fact, diffuse metal ion binding often plays a dominant role in stabilizing small RNA tertiary structures (*45*). To visualize this effect for the hammerhead ribozyme, we have calculated the electrostatic surface potentials and metal ion distributions around the hammerhead ribozyme at bulk concentrations of 100 mM Na^{+} and 10 mM Mg^{2+}, using the nonlinear Poisson−Boltzmann (NLPB) equation (*36*, *37*) (see Materials and Methods). Figure 9 shows the 2.5 M Mg^{2+} isoconcentration contour maps around the NMR structure (*35*) and the crystal

structure (*6*). The higher charge density associated with the more compact crystal structure leads to accumulation of Mg^{2+} concentrations higher than those observed for the NMR structure, especially around the center of the junction and in the minor grooves. It is this enhanced diffuse metal ion binding which is predicted to stabilize the tertiary folded (crystal structure-like) conformation over any unfolded (NMR structure-like) conformations (*45*).

To understand why only nonphysiologically high Mg^{2+} concentrations seem to mediate the folding of stems I and II into the catalytically active structure, we must turn our attention to the natural sequence context of hammerhead ribozymes. It has been recently revealed that most naturally occurring hammerhead ribozymes contain specific kissing-loop interactions between stems I and II (*46*). When tested for their catalytic activity, such kissing-loop-containing hammerhead ribozymes appear to have greatly accelerated catalytic activities at physiological Mg^{2+} concentrations (*46*). Furthermore, HHα activity has been observed to be dependent on the length of stem I (*25*). As stems I and II are in van der Waals contact, even in a short-stemmed hammerhead crystal structure (*6*), this length dependence may indicate increased steric clash between extended stems in the catalytically active structure. Likewise, bulky 2′ modifications inhibit catalysis when incorporated in certain positions of stems I and II which should, according to the crystal structure, be able to accommodate them (*47*). All of these observations, together with our Mg^{2+}-dependent tr-FRET and cleavage data, lead us to propose the following ideas. First, the kissing-loop interaction in natural hammerhead ribozymes orients stems I and II in a conformation that favors access to the transition state. Second, this conformation is globally similar to but locally distinct from the Y-shaped crystal structure. Differences may include, for example, twisting of stems I and II relative to their crystal structure positions. Third, the loss of the kissing-loop interaction, due to truncation of the naturally occurring hammerhead ribozymes (*48*−*50*), is offset by diffusely bound Mg^{2+} ions, which function by increasing the probability of formation of a properly aligned catalytic core.

Many heretofore seemingly controversial, or not fully explained, observations about the hammerhead ribozyme may potentially be reconciled on the basis of the above ideas, as follows.

(i) The enhanced flexibility of HHα may be the reason for its higher activity at low Mg^{2+} concentrations. Greater flexibility leads to easier access to all conformations, including the transition state. Therefore, the Mg^{2+} binding energy necessary to twist HHα into the active conformation is lower, effectively decreasing the Mg^{2+} concentration requirement for activation.

(ii) The high catalytic activity of the hammerhead ribozyme is observed at molar concentrations of monovalents, such as Na^+ and NH_4^+ (*19*−*21*). This is consistent with a primary function of diffusely bound (rather than site-bound) cations in increasing the probability of formation of a properly aligned catalytic core.

(iii) The hammerhead ribozyme can function under a variety of conditions, possibly using numerous pathways to reach a catalytically active state. In the crystal, high pH and saturating cation concentrations seem to allow necessary local adjustments (*17*, *22*). With double (R_p)-phosphorothioate modifications in the presence of Cd^{2+} (*14*), the short residence time of the Cd^{2+} ions [in the millisecond range (*51*)] may allow them to associate with both sulfur atoms, aiding in the formation of the catalytically active structure [which occurs on the minute time frame of catalysis; this scenario is therefore compatible with but not dependent on the controversial simultaneous ligation of both sulfurs, 20 Å apart in the crystal structure, by a single Cd^{2+} ion (*14*, *15*)]. At high Mg^{2+} concentrations, diffusely bound Mg^{2+} ions aid the ribozyme in rearranging to an active form (this work). And, finally, in naturally occurring ribozymes at physiological Mg^{2+} concentrations, "kissing-loop" tertiary interactions may stabilize the proper catalytic structure (*46*).

Recently, indirect evidence from mechanistic studies has suggested that the initially formed ribozyme−substrate complex (Rz·S) may be in equilibrium with an alternate active conformation (Rz·S*) (*47*), an assumption similar to the one we used for interpreting our Mg^{2+} titration data (see eq 4). In addition, the ribozyme−product complex has been proposed to change conformation following cleavage and prior to product release (*40*), and we here have presented, to our knowledge, the first direct evidence of such an alternate product complex conformation (Figure 7). Future studies on hammerhead ribozymes containing a kissing-loop interaction between stems I and II will directly illuminate the role that this tertiary contact plays in folding and function of this small and well-studied yet still intriguingly elusive catalytic RNA.

ACKNOWLEDGMENT

We thank Vinod Misra for help with preparing Figure 9, all members of the Walter laboratory as well as Vincent Pecoraro for stimulating discussions, Tom Kerppola for making his FluorImager for gel mobility FRET assays available to us, Art Pardi for providing us with the coordinates of his NMR structure of the hammerhead ribozyme, and Steve Katnik for help with maintaining the Tsunami laser system.

REFERENCES

1. Long, D. M., and Uhlenbeck, O. C. (1993) *FASEB J. 7*, 25−30.
2. Symons, R. H. (1997) *Nucleic Acids Res. 25*, 2683−2689.
3. Epstein, L. M., and Gall, J. G. (1987) *Cell 48*, 535−543.
4. Pley, H. W., Flaherty, K. M., and McKay, D. B. (1994) *Nature 372*, 68−74.
5. Scott, W. G., Finch, J. T., and Klug, A. (1995) *Cell 81*, 991−1002.
6. Scott, W. G., Murray, J. B., Arnold, J. R. P., Stoddard, B. L., and Klug, A. (1996) *Science 274*, 2065−2069.
7. Tuschl, T., Gohlke, C., Jovin, T. M., Westhof, E., and Eckstein, F. (1994) *Science 266*, 785−789.
8. Bassi, G. S., Murchie, A. I., Walter, F., Clegg, R. M., and Lilley, D. M. (1997) *EMBO J. 16*, 7481−7489.
9. Bassi, G. S., Mollegaard, N. E., Murchie, A. I., von Kitzing, E., and Lilley, D. M. (1995) *Nat. Struct. Biol. 2*, 45−55.
10. Amiri, K. M., and Hagerman, P. J. (1996) *J. Mol. Biol. 261*, 125−134.
11. Ruffner, D. E., Stormo, G. D., and Uhlenbeck, O. C. (1990) *Biochemistry 29*, 10695−10702.
12. Wedekind, J. E., and McKay, D. B. (1998) *Annu. Rev. Biophys. Biomol. Struct. 27*, 475−502.
13. McKay, D. B. (1996) *RNA 2*, 395−403.
14. Wang, S., Karbstein, K., Peracchi, A., Beigelman, L., and Herschlag, D. (1999) *Biochemistry 38*, 14363−14378.
15. Murray, J. B., and Scott, W. G. (2000) *J. Mol. Biol. 296*, 33−41.
16. Hammann, C., and Lilley, D. M. (2002) *ChemBioChem 3*, 690−700.

17. Murray, J. B., Szoke, H., Szoke, A., and Scott, W. G. (2000) *Mol. Cell 5*, 279−287.
18. Dahm, S. C., Derrick, W. B., and Uhlenbeck, O. C. (1993) *Biochemistry 32*, 13040−13045.
19. Murray, J. B., Seyhan, A. A., Walter, N. G., Burke, J. M., and Scott, W. G. (1998) *Chem. Biol. 5*, 587−595.
20. O'Rear, J. L., Wang, S., Feig, A. L., Beigelman, L., Uhlenbeck, O. C., and Herschlag, D. (2001) *RNA 7*, 537−545.
21. Curtis, E. A., and Bartel, D. P. (2001) *RNA 7*, 546−552.
22. Murray, J. B., Dunham, C. M., and Scott, W. G. (2002) *J. Mol. Biol. 315*, 121−130.
23. Hampel, K. J., and Burke, J. M. (2003) *Biochemistry 42*, 4421−4429.
24. Clouet-d'Orval, B., and Uhlenbeck, O. C. (1996) *RNA 2*, 483−491.
25. Clouet-d'Orval, B., and Uhlenbeck, O. C. (1997) *Biochemistry 36*, 9087−9092.
26. Walter, N. G., Burke, J. M., and Millar, D. P. (1999) *Nat. Struct. Biol. 6*, 544−549.
27. Pereira, M. J., Harris, D. A., Rueda, D., and Walter, N. G. (2002) *Biochemistry 41*, 730−740.
28. Walter, N. G., Harris, D. A., Pereira, M. J., and Rueda, D. (2002) *Biopolymers 61*, 224−242.
29. Bassi, G. S., Mollegaard, N. E., Murchie, A. I., and Lilley, D. M. (1999) *Biochemistry 38*, 3345−3354.
30. Walter, N. G. (2001) *Methods 25*, 19−30.
31. Walter, N. G., and Burke, J. M. (2000) *Methods Enzymol. 317*, 409−440.
32. Walter, N. G., Hampel, K. J., Brown, K. M., and Burke, J. M. (1998) *EMBO J. 17*, 2378−2391.
33. Ramirez-Carrozzi, V. R., and Kerppola, T. K. (2001) *Methods 25*, 31−43.
34. Mueller, F., and Brimacombe, R. (1997) *J. Mol. Biol. 271*, 524−544.
35. Bondensgaard, K., Mollova, E. T., and Pardi, A. (2002) *Biochemistry 41*, 11532−11542.
36. Sharp, K. A., and Honig, B. (1990) *Annu. Rev. Biophys. Biophys. Chem. 19*, 301−332.
37. Misra, V. K., and Draper, D. E. (2000) *J. Mol. Biol. 299*, 813−825.
38. Nicholls, A., Sharp, K. A., and Honig, B. (1991) *Proteins 11*, 281−296.
39. Walter, N. G., and Burke, J. M. (1997) *RNA 3*, 392−404.
40. Blount, K. F., and Uhlenbeck, O. C. (2002) *Biochemistry 41*, 6834−6841.
41. Harris, D. A., Rueda, D., and Walter, N. G. (2002) *Biochemistry 41*, 12051−12061.
42. Fersht, A. (1999) *Structure and Mechanism in Protein Science*, Freeman, New York.
43. Murray, J. B., Terwey, D. P., Maloney, L., Karpeisky, A., Usman, N., Beigelman, L., and Scott, W. G. (1998) *Cell 92*, 665−673.
44. Pyle, A. M. (2002) *J. Biol. Inorg. Chem. 7*, 679−690.
45. Misra, V. K., and Draper, D. E. (2002) *J. Mol. Biol. 317*, 507−521.
46. Khvorova, A., Lescoute, A., Westhof, E., and Jayasena, S. D. (2003) *Nat. Struct. Biol.* (in press).
47. Blount, K., Grover, N., Mokler, V., Beigelman, L., and Uhlenbeck, O. (2002) *Chem. Biol. 9*, 1009−1016.
48. Buzayan, J. M., Gerlach, W. L., and Bruening, G. (1986) *Nature 323*, 349−353.
49. Uhlenbeck, O. C. (1987) *Nature 328*, 596−600.
50. Bruening, G. (1989) *Methods Enzymol. 180*, 546−558.
51. Pecoraro, V. L., Hermes, J. D., and Cleland, W. W. (1984) *Biochemistry 23*, 5262−5271.
52. Hertel, K. J., Pardi, A., Uhlenbeck, O. C., Koizumi, M., Ohtsuka, E., Uesugi, S., Cedergren, R., Eckstein, F., Gerlach, W. L., Hodgson, R., et al. (1992) *Nucleic Acids Res. 20*, 3252.

BI0347757